A spectroscopic study of CH3F isolated in rare gas matrices

V. A. Apkarian and Eric Weitz

Citation: The Journal of Chemical Physics **76**, 5796 (1982); doi: 10.1063/1.442977
View online: http://dx.doi.org/10.1063/1.442977
View Table of Contents: http://scitation.aip.org/content/aip/journal/jcp/76/12?ver=pdfcov
Published by the AIP Publishing

A spectroscopic study of CH_3F isolated in rare gas matrices

V. A. Apkarian [a] and Eric Weitz [b]

Department of Chemistry, Northwestern University, Evanston, Illinois 60201
(Received 30 November 1981; accepted 11 March 1982)

The hindered rotational/librational motion of symmetric top molecules isolated at substitutional sites in rare gas matrices is considered. It is shown that the dominant perturbation of the free rotor states is due to the reorientational forces of the cage atoms. An electrostatic model for symmetric top molecules trapped in octahedral fields that hinder the molecular tumbling motion is developed. The model is successfully applied to the qualitative interpretation of experimentally observed line shapes, linewidths, and spectral shifts of the ν_3 mode of CH_3F isolated in rare gas matrices. Exact quantitative predictions are not made due to the many model parameters, however, the spectra are compatible with a minimum barrier to tumbling of approximately 80 cm^{-1} and are compatible with free spinning motion. A complete analysis of the spectra requires the consideration of dynamic perturbations as well as possible sources of dynamic line broadening. The role of rotation-translation coupling is also explored. Experimental studies have provided a direct measure of the ν_3 intergrated absorption coefficient from which a radiative lifetime of $\tau = 82 \pm 10$ ms is obtained. Direct observation of $2\nu_3$ yields the first anharmonicity constant $\omega_e\chi_e = 8.05 \pm 0.05$ cm^{-1}. Studies of matrices "capped" with pure rare gas have provided an insight as to the dynamics of aggregation with the conclusion that aggregation occurs at surfaces and grain boundaries. An absorption at 1034 cm^{-1} is assigned to molecules trapped in these locations. Implications with respect to energy transfer processes in these systems are also discussed.

INTRODUCTION

Studies of vibrational energy transfer and relaxation processes of ground electronic state molecules in solid media, such as low temperature matrices, are fairly recent.[1-3] The only polyatomic molecules which have been subjected to detailed experimental studies are the symmetric tops: NH_3[4], CH_3F[5-7] and CD_3F.[8] Information about the interactions of a molecule with its trap site and its overall dynamics, including an understanding of degrees of freedom other than internal vibrations, is important for a complete grasp of vibration–vibration ($V-V$) energy transfer and relaxation processes. Much of this information can, at least in principle, be gotten from spectroscopic studies. We have previously reported on laser induced fluorescence studies of vibrational energy transfer in matrix isolated CH_3F.[6] In the present paper, we report on spectroscopic studies of the same system in an effort to extract complimentary information about the molecular dynamics of this system.

Both theoretical and experimental studies indicate that molecular rotations/librations play an important role in vibrational energy transfer processes of matrix isolated molecules by coupling the molecular vibrations to lattice phonons.[1-10] This effect is particularly important in the deactivation of molecular vibrations. Thus, it is crucial to understand the status of molecular rotations in the matrix cage. The librational motion of diatomics, such as hydrogen halides, has been studied spectroscopically and interpreted by various theoretical models.[11] Interpretation of infrared spectra of polyatomic molecules has been less rigorous for two main reasons: the lack of high resolution spectra and the lack of an advanced model of hindered polyatomic rotors. High resolution spectra are necessitated by the larger moments of inertia that generally occur in polyatomics. It can also be argued that, for large molecules possessing large moments of inertia, dynamic perturbations on the molecular rotations are not as important as perturbations due to reorientational forces and therefore electrostatic models may be better suited to describe the behavior of these systems. A crystal field model was first introduced by Devonshire to treat the problem of a diatomic rotor in an octahedral field.[12] This model has not been previously extended to the case of polyatomics even though the problem is well defined, at least for systems of high symmetry.[13]

Methyl monohalides in condensed media have been the subject of numerous spectroscopic studies.[14-27] Based on the observation that in solution their perpendicular bands approximately follow the contours of the gas phase bands, it has been concluded that these molecules undergo a somewhat hindered rotation about their C_3 axes in the liquid phase.[14-19] A tumbling motion for CH_3F in liquid solutions is inferred from the observation that its parallel bands are also broad.[18] No evidence of rotations was found in a study of CH_3F isolated in Ar and CH_4 matrices at 20 K and in neat CH_3F matrices.[25] Contrasted with the above studies were the conclusions of a more recent matrix study: that CH_3F in Kr matrices is quite free to rotate at 25 K and a shoulder observed in a 1.5 mm thick, 500:1 Kr:CH_3F matrix was assigned to a "librational satellite" from which a 3–6 cm^{-1} barrier to rotation was derived.[26] The latter assignment was reportedly based on Pauling's and Devonshire's models of hindered linear rotors.[12,28] Based on similar observations and arguments, these authors assigned rotational barriers to CH_3F and CD_3F isolated in various rare gas matrices; for CH_3F, these values range from < 2 cm^{-1} in Xe to 10.9 ± 1 cm^{-1} in Ar.[26] In a different and a yet more recent study, other authors conclude that the rotations of CH_3F and CD_3F are completely frozen in Ar and Kr matrices.[27] It should be obvious from this compilation that the question of rotation of halomethanes in condensed media is,

[a] Present address: Dept. of Chemistry, Cornell University, Ithaca, N.Y. 14853.
[b] Alfred P. Sloan Fellow.

 0021-9606/82/125796-16$02.10

at best, a confused issue.

In what follows, we first discuss the applicability and then present the predictions of the Devonshire model extended to treat symmetric top molecules. Both energy levels and transition moments of hindered symmetric tops are calculated from which predicted infrared spectra are constructed. The results are applicable to any symmetric top molecule. However, we will concentrate on applications to CH_3F. The experimental results of spectroscopic studies will be reported concentrating on the ν_3 region of CH_3F isolated in Kr matrices. The spectra were obtained with a Fourier transform infrared spectrometer which is capable of 0.06 cm^{-1} resolution. It will be shown that experimental results can be at least qualitatively explained by the predictions of the model. A preliminary report of this work has been previously presented.[6(b),6(c)]

THEORETICAL CONSIDERATIONS

Numerous investigators have considered the theory for rotations of molecules trapped in rare gas lattices. Two major perturbations of free rotor states are considered: (a) the electrostatic barrier exerted by the cage atoms—the crystal field model; (b) the coupling between molecular translations and rotations–the RTC model. The Hamiltonian which includes both of these effects can be written as

$$H = H(t) + H(r) + H(l) + H(r - t) \ . \tag{1}$$

$H(t)$ describes the motion of the molecular center of mass in the lattice cell and can be identified as the harmonic oscillator Hamiltonian which gives rise to local or resonant phonons, $H(r)$ is the free rotor Hamiltonian, $H(l)$ is the potential exerted by the lattice atoms on the free rotor, and $H(r-t)$ describes the coupling between translational and rotational motions of the molecule.

The crystal field models consider only the second and third terms of Eq. 1. Such a model was first presented by Pauling for the case of a diatomic molecule rotating in a cylindrical well.[28] He developed a two-dimensional model for a plane rotor in a potential expressed as $V_0(1 - \cos 2\theta)$; where V_0 is the barrier to end-over-end rotation and θ is the angle about the axis perpendicular to the internuclear axis. In the limit of large V_0 and large moments of inertia, the molecular motion reduces to that of a two-dimensional harmonic oscillator with energy levels

$$E_n = (n+1)\, h\nu_0, \quad n = 0, 1, 2 \cdots, \text{ and } \nu_0 = \frac{1}{\pi}\left(\frac{V_0}{I}\right)^{1/2} , \tag{2}$$

where I is the molecular moment of inertia.

The first theoretical model utilizing a three-dimensional potential was presented by Devonshire, who investigated the Schrödinger equation of a linear rotor in an octahedral field.[12] The potential is expanded in surface harmonics of fourth degree and can be expressed as

$$V = -C[\tfrac{1}{8}(3 - 30\cos^2\theta + 35\cos^4\theta + 5\sin^4\theta\cos 4\phi)] \ , \tag{3}$$

where C is termed the height of the rotational barrier and used strictly as a parameter. C is equivalent to the K used in Devonshire's formulation. The determinantal equations are then solved in the basis set of the free rotor states after symmetry factorization and truncation. The energy levels thus obtained are tabulated as a function of reduced barrier height C/B, where B is the rotational constant of the molecule.

The nature of the barrier to rotation was investigated by Flygare.[13] He ignores repulsive interactions due to the overlap of electronic wave functions of the molecule and cage atoms based on the argument that most vibronic transitions in condensed phases are red shifted from their gas phase values. Thus, the dominant contributions to the interaction potential between a molecule whose center of mass is fixed at the substitutional site of an fcc lattice is determined to be the hexadecapole coupling constants $\sum_k \Gamma_k^4$, which are products of the molecular hexadecapoles, and the fourth gradient of the electric potential at the molecular center of mass, summed over all lattice charges. The nonvanishing terms in the summation over k are determined by the molecular symmetry. In addition to this interpretation of the rotational barrier, Flygare provides a general formalism for the treatment of molecules of high symmetry trapped in normalized octahedral fields.[13]

Crystal field model predictions were applied to interpret experimental condensed phase spectra with limited success.[29,11] In the case of hydrogen halides, a more consistent interpretation of spectroscopic data could be obtained by consideration of the dynamic perturbations on the molecular rotations, hence, the introduction of the rotation-translation coupling (RTC) model which was also able to predict the correct isotopic substitution effects for the frequencies of rotational transitions.[30]

In the RTC model, the first, second, and fourth terms of Eq. (1) are retained and the shifts of the free rotor transitions and their relative intensities are calculated by perturbation theory. The coupling between $H(t)$ and $H(r)$ is basically due to the difference d between the molecular center of mass and the center of electrical interaction. The coupling will also depend on the difference in rotational and translational energies of the system. In the case of hydrogen halides, due to the large asymmetry of nuclear masses, a large value of d is expected. While d cannot be reliably calculated, it can be determined from experimental data. For HCl, $d \simeq 0.095$ Å is determined experimentally and found to be the same in all rare gas matrices.[11] In the case of molecules with centers of mass very near their geometric centers, a smaller value of d would be expected. Furthermore, while for all hydrogen halides the rotational spacings are comparable to the translational energy levels, in the case of polyatomics with small B values this is not true. The change in rotational energy predicted by the RTC model to second order in d and for the harmonic oscillator cell model is given as

$$\frac{\Delta E(J)}{hcB} = \frac{md^2\xi}{2I}\left[1 - \frac{2\xi(J^2+J+1) - 4J(J+1)}{(\xi - 2J)(\xi + 2J + 2)}\right], \tag{4}$$

where B is the rotational constant, m is the molecular mass, d is the distance between the center of mass and center of interaction, I is the moment of inertia, and $\xi = \nu/B$, where ν is the frequency of oscillation of the solute molecule in its cage and can be calculated as[30]

$$\nu = \frac{1}{\pi a c}\left(\frac{12\epsilon}{m}\right)^{1/2}\left[44\left(\frac{\sigma}{a}\right)^{12} - 10\left(\frac{\sigma}{a}\right)^{6}\right]^{1/2}, \tag{5}$$

where a is the nearest neighbor distance, and ϵ and σ are the Lennard-Jones parameters.[31] For CH_3F in Kr matrices, $\nu = 69.7\ cm^{-1}$ is calculated (σ and ϵ values of 3.62 Å and 170 K for Kr[32] and 3.73 Å and 333 K for CH_3F[33] were used.)

In the case of CH_3F, one expects $d < 0.095$ Å due to the fact that the molecular center of mass is nearer the molecule's geometric center than in the case of HCl. However, even if $d = 0.095$ Å is used, very small shifts would be predicted for the energies of the lowest rotational levels. As an illustration, the $R(0)$–$P(1)$ separation of $4B$ in the gas phase would be contracted by ~1.6%. Thus, only high lying J states would be appreciably affected in this model. At low temperatures, where only the lowest rotational states are populated, the shape of the rovibrational envelope would be essentially unaltered from that of the free rotor spectrum. This is contrary to experimental observations where very narrow rovibrational envelopes are observed. These envelopes are well predicted by the crystal field model without the introduction of any rotation-translation coupling. This will be demonstrated below.

CRYSTAL FIELD MODEL FOR A HINDERED SYMMETRIC TOP ROTOR

According to Flygare's formalism, the Hamiltonian matrix of a symmetric top in an octahedral field can be written as

$$\langle H\rangle = BJ(J+1) + (A-B)K^2 + V^J\langle JKM|D^4_{00} + \left(\frac{5}{14}\right)^{1/2}(D^4_{04} + D^4_{0-4})|J'K'M'\rangle + \left(\frac{2}{7!}\right)^{1/2} V^K\langle JKM|D^4_{30} + \left(\frac{5}{14}\right)^{1/2}(D^4_{34} + D^4_{3-4})|J'K'M'\rangle, \tag{6}$$

where V^J and V^K correspond to $(\sqrt{7}/6)\langle l|x^4|l\rangle H_d(0)$ and $(\sqrt{7}/6\langle l|x^4|l\rangle H_d(3)$ of Ref. 13. $D^J_{KM}(\alpha\beta\gamma)$ functions are the conventional rotational matrices and Ψ_{JKM} is the symmetric top rotational wave function and can be expressed as[34]

$$\Psi_{JKM} = \left(\frac{2J+1}{8\pi^2}\right)^{1/2} D^J_{-K-M}. \tag{7}$$

After substituting Eq. (7) into Eq. (6), each term of the perturbation Hamiltonian becomes the product of three $D(\alpha\beta\gamma)$ functions which can be evaluated very conveniently by Clebsch–Gordan coefficients.[34] Thus, Eq. (6) can be recast as

$$\langle H\rangle = BJ(J+1) + (A-B)K^2 + \left(\frac{2J+1}{2J'+1}\right)^{1/2} V^J c(J,4,J',-K,0,-K')\{c(J,4,J',-M,0,M') + \left(\frac{5}{14}\right)^{1/2}[(c(J,4,J',-M,4,-M') + c(J,4,J',-M,-4,-M')]\} + \left(\frac{2}{7!}\right)^{1/2}\left(\frac{2J+1}{2J'+1}\right)^{1/2} V^K c(J,4,J',-K,3,-K') \times \{c(J,4,J',-M,0,-M') + \left(\frac{5}{14}\right)^{1/2}[c(J,4,J',-M,3-M') + c(J,4,J',-M,-3,-M')]\}. \tag{8}$$

V^J of Eq. (6) is defined such that when K states are dropped, the Hamiltonian corresponds exactly to the one defined by Devonshire with the identification of V^J as the potential barrier height K defined by Devonshire. To avoid confusion, any future reference to K will denote the K quantum number with V^J and V^K denoting barrier heights. When K is set to zero and J states up to 12 are used in the computation, good agreement is obtained between calculated eigenvalues and those tabulated by Devonshire or Sauer.[12,35] Inspection of Eq. (8) indicates that V^J terms vanish unless $K = K'$, and therefore produces no K state mixing. Thus, V^J can be regarded as the barrier to the tumbling motion of the molecule, i.e., rotation of the symmetry axis. Mixing of K states is due only to the V^K terms and therefore V^K is identified with the barrier to spinning, rotation about the C_3 symmetry axis. Since computation of the different hexadecapole moments of the molecule cannot be accomplished with any accuracy, V^J and V^K will be used strictly as parameters; however, $V^K \ll V^J$ is expected based on geometric considerations alone.

The matrix defined by Eq. (8) is of infinite order and an appropriate truncation is necessary for its solution. Unfortunately, matrices of very large dimension are necessary if the complete Hamiltonian is to be accurately diagonalized even for small values of V^J and V^K. As an example, if $K = -4, \cdots, 4$ and $J = 0, \cdots, 8$ are included, which would be satisfactory for V^J, $V^K \sim 0$–$10\ cm^{-1}$ (in the case of CH_3F) 1083 JKM states must be considered. Thus, as a first approximation, $V^K = 0$ is assumed. Since the remaining Hamiltonian does not produce any K state mixing, the matrix can be block diagonalized for each K state. This factorization is

TABLE I. Reduced energy of states as a function of reduced potential.

			Reduced energy $(E/B)^f$			
a	J^b	g^c	$V^J=0$	$V^J\simeq 10B^d$	$V^J\simeq 50B^d$	$V^J\simeq 100B^e$
1	0	1	0	−1.045	−21.45	−58.09
2	1	3	2	0.636	−21.32	−58.06
3	2	2	6	2.345	−21.24	−58.06
4	2	3	6	7.488	3.434	−18.68
5	3	1	12	15.48	24.55	18.70
6	3	3	12	10.61	4.344	−18.54
7	3	3	12	12.28	4.780	−18.51
8	4	1	20	17.99	17.74	11.80
9	4	2	20	19.99	21.04	13.67
10	4	3	20	18.39	5.948	−18.38
11	4	3	20	22.29	27.88	19.36
12	5	2	30	31.32	31.25	19.75
13	5	3	30	28.03	22.68	13.47
14	5	3	20	28.96	25.74	16.69
15	6	1	42	40.72	33.30	18.56
16	6	2	42	40.01	31.35	16.97

[a]State designation number used in the text.
[b]Correlated free rotor J state.
[c]Degeneracy.
[d]Energies obtained from a basis set that contained J states up to $J=12$.
[e]Energies obtained from a basis set that contained J states up to $J=16$.
[f]Only the lowest 16 states are reported in the actual calculations ~80 states are included.

sufficient to yield manageable size matrices in the range of potentials to be considered (the largest computed matrix was 320×320). Additionally, since we are interested in molecular motion at low temperatures, only the $K=0$, 1, and 2 blocks need be considered. Thus, each block is diagonalized to yield the energy levels of a particular K manifold at a given value of V^J. The eigenvectors ϕ_i,

$$\phi_i=\sum_{JKM} a_{iJKM}|JKM\rangle \tag{9}$$

are then computed and used to calculate the dipole transition moments $\langle\mu_{ij}\rangle^2$ as

$$\langle\mu_{ij}\rangle^2=(\langle\phi_i|D^1_{00}|\phi_j\rangle)^2+(\langle\phi_i|D^1_{01}|\phi_j\rangle)^2+(\langle\phi_i|D^1_{0-1}|\phi_j\rangle)^2 . \tag{10}$$

Clearly, the selection rules $\Delta K=0$ for parallel bands and $\Delta K=\pm 1$ for perpendicular bands are preserved and therefore, in the case of parallel bands, only transitions within a K block need be considered.

As previously discussed for $K=0$, the problem reduces to that of a linear rotor in an octahedral field and conclusions derived in previous studies are applicable. The most comprehensive tabulation of energy levels as a function of V^J/B are presented by Sauer who also discusses the convergence of eigenvalues as a function of the basis set.[35] A plot of different transition moments as a function of V^J/B is presented by Beyeler.[36] In Table I, 16 of the lowest states in the $K=0$ manifold are presented at four different potentials and their transition moments are presented in Table II.

For $K=1$, the lowest energy levels roughly parallel those of $K=0$ (see Fig. 1). This similarity in behavior of eigenvalues in different K manifolds is not reflected in the eigenvectors. The most important contrast between eigenvectors of states $K\neq 0$ and those of $K=0$ is the loss of parity conservation: while for $K=0$, odd J states mix only with odd J states, and even J states only mix with even ones, as a result of the loss of the molecule-cage center of symmetry, in $K\neq 0$, odd and even states are mixed. As a consequence, Q type transitions are allowed in $K\neq 0$ manifolds.

Rovibrational spectra based on this model of hindered rotations can only be constructed if the values of V^J are known for both the ground and the particular excited vibrational levels. In previous calculations and interpretations, it has been implicitly assumed that the same rotational barrier describes the motion in both these states.[11] This assumption is not necessarily justified. The molecular multipoles depend on the nuclear separations which, in turn, depend on the vibrational states of the molecule. Furthermore, repulsive interactions are expected, in general, to increase as a function of vibrational excitation. However, a theoretical determination of V^J as a function of vibrational excitation is not straightforward and more realistically should be left as a parameter to be determined from experimental data. Thus, for illustrative purposes, the barriers in the ground and first excited states are initially assumed to be the same and spectra generated for V^J

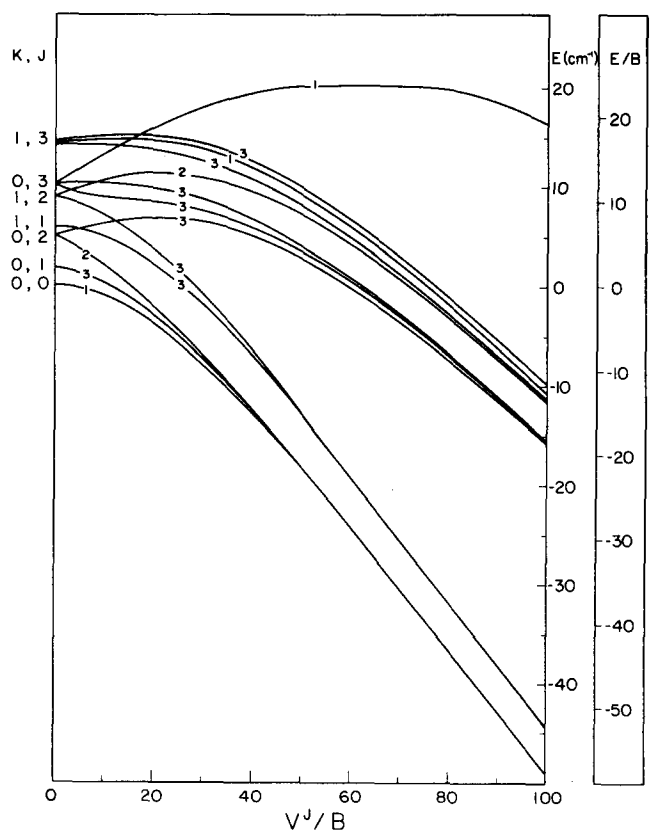

FIG. 1. Plotted is the dependence of the energy of some of the lower vibrational J, K states as a function of the reduced barrier (V^J/B). The free rotor J, K states are indicated on the left. The J multiplicities are indicated along the curves. The K multiplicity due to $\pm K$ states is not indicated. Energy (E) and reduced energy (E/B) are indicated on the right.

TABLE II. Transition moments[a] of the $K=0$ manifold.

	1	2	3	4	5	6	7	8	9	10	11	12	13
	...	9.72(−1)	...	...	...	2.45(−2)	...	...	...	...	...	...	2.74(−3)
1	...	9.30(−1)	...	...	...	6.64(−2)	...	...	...	...	...	...	4.72(−3)
	...	9.48(−1)	...	...	...	4.92(−2)	...	...	...	...	...	...	1.13(−3)
		...	1.31	6.79(−1)	...	...	...	4.66(−3)	7.99(−4)	3.40(−2)	2.75(−4)	...	...
2		...	1.84	1.19(−1)	...	...	...	2.17(−3)	1.21(−3)	1.00(−1)	1.89(−4)	...	...
		...	1.90	7.38(−2)	...	...	...	4.42(−4)	5.56(−4)	7.60(−2)	...	...	...
			...	...	...	4.22(−1)	2.67(−1)	...	...	...	...	...	...
3			...	...	...	5.52(−2)	1.09(−1)	...	...	...	...	...	9.27(−4)
			...	...	...	2.44(−2)	7.36(−2)	...	...	...	...	...	1.27(−3)
				...	3.25(−1)	9.80(−1)	1.01	...	...	...	...	2.65(−3)	1.73(−4)
4				...	9.65(−2)	1.34	1.28	...	...	...	...	2.7(−2)	4.68(−2)
				...	5.15(−2)	7.35	1.35	...	...	...	...	2.50(−2)	6.89(−2)
					...	...	...	...	...	...	6.73(−1)	...	...
5					...	...	...	...	...	...	8.55(−1)	...	...
					...	...	...	...	...	...	8.43(−1)	...	...
						...		4.56(−1)	4.63(−2)	7.78(−1)	9.57(−2)	...	...
6						...		1.80(−1)	6.58(−2)	1.13	8.41(−2)	...	...
						...		6.99(−2)	3.96(−3)	1.32	7.85(−2)	...	...
							...	...	6.11(−1)	6.22(−1)	4.89(−1)	...	...
7							...	...	2.39(−1)	1.16	1.50(−1)	...	...
							...	...	1.26(−1)	1.32	8.03(−2)	...	...
								...	...	...	...	...	5.33(−1)
8								...	...	...	...	...	7.93(−1)
								...	...	...	...	...	8.38(−1)
									...	...	...	...	1.71(−1)
9									...	...	...	...	4.66(−1)
									...	...	...	...	9.79(−1)
										...	...	2.14(−1)	6.85(−1)
10										...	...	1.12(−1)	2.69(−1)
										...	...	7.59(−2)	9.79(−2)
											...	6.89(−1)	1.53(−2)
11											...	1.13	...
												1.60	5.39(−4)
12													
13													

[a]The moments are summed over both initial and final state degeneracies in order to yield a symmetric matrix. Thus, a transition from states 4–7 is simply given as $A/Q \exp[(E_0 - E_4)/kT]$ where A is the entry in the matix, E_4 is the energy of state 4 and E_0 is the lowest rotational energy level in the whole manifold, and Q is $\Sigma_i \exp[E_0 - E_i)/kT]$. All tabulated moments were calculated from a basis set that contains free rotor states up to $J=12$. The three entries correspond to the moments for $V^J = 10B$, $50B$, and $100\,B$. Only moments larger than 10(−4) are reported. The number in parenthesis is the power of ten to which the number to its left should be raised.

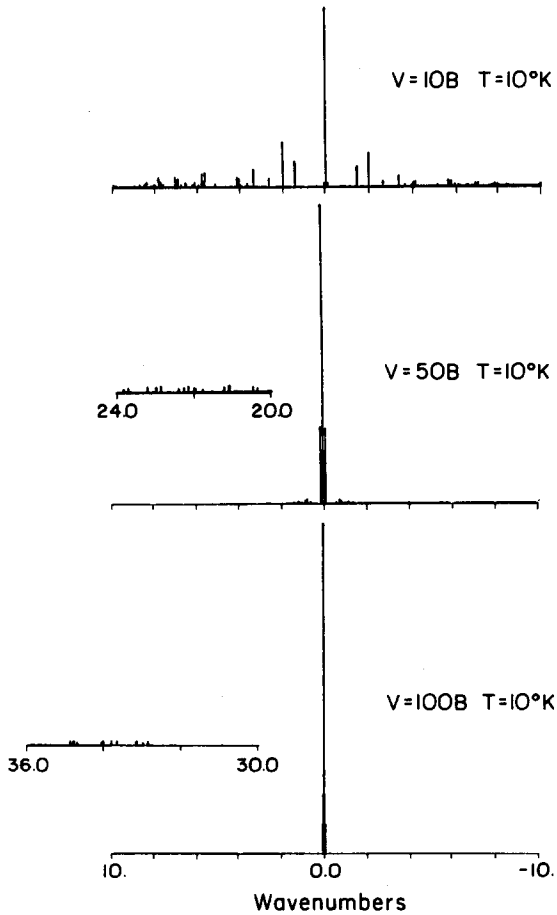

FIG. 2. Generated stick spectra for a symmetric top molecule with $V^K=0$, $V^J=V^{J'}=V$, $A=5.12$ cm^{-1}, $B=0.851$ cm^{-1}, and the temperature as indicated. Insets are expanded by a factor of 2.

$=10B$, $50B$, and $100B$ for a parallel transition, using $B=0.85$ and $A=5.12$ cm^{-1} for both the ground and excited vibrational levels are shown in Fig. 2.

At 10 K and for all values of V^J, the dominant contribution to the spectral intensity in Fig. 2 is due to $K=1$ transitions. This is caused by the fact that though transition moments of the $K=1$ and $K=0$ states are comparable, $K\neq 0$ states are doubly degenerate and therefore for values of A comparable to or small with respect to KT (which is the case for CH_3F even at 10 K), the populations in low lying J states of the $K=1$ manifold can be larger than those of $K=0$. It is important to note the very strong Q lines, which are sums of rovibrational transitions with the same initial and final rotational states. Such transitions are not allowed for $K=0$, where due to conservation of the molecule-cage center of symmetry, all rotational states can be identified as odd or even. It follows that for $A \gg KT$ or equivalently at very low temperatures, transitions in $K\neq 0$ manifolds and therefore the Q lines will vanish.

Finally, it can be seen that for small values of V^J, a complex rotational structure is to be expected for CH_3F even at 10 K. At moderately high potentials $V^J=50B$, the spectrum is greatly simplified. The spectrum is composed of some intense lines centered about the Q line and a weaker feature blue shifted by ~ 20 cm^{-1}. The spread of the center lines is determined by the spacing among the lowest states of the $K=0$ and $K=1$ manifolds; states that can be correlated to the free rotor states $J=0, 1$, and 2 of $K=0$ and $J=1$ and 2 of $K=1$. The center lines are spread over a ~ 1 cm^{-1} region when a basis set of 81 JKM states is used, ~ 0.252 cm^{-1} when 169 JKM states are used and ~ 0.250 cm^{-1} when 289 JKM states are used. Whether these lines could be separated by high resolution spectroscopy would depend on the width of the individual lines. In the case of $V^J=100B$, the blue satellite is removed by ~ 34 cm^{-1} from the Q line and is very weak. The spread of the center lines is over 0.17 cm^{-1} when 169 states are used and 0.018 cm^{-1} when 289 states are used. For all practical purposes, at this potential the $K=0$ states that can be correlated to $J=0$, $J=1$, and $J=2$ are degenerate and therefore the spectrum should show an even stronger Q line. The blue satellites are usually termed "librational satellites," the indicated spread of these lines on the constructed spectra are due to lack of complete convergence of the upper states involved in these transitions. In the limit of a very large V^J, strictly librational motion, each K manifold will produce a single spectroscopic line.

The coupling between hindered rotations and translation of the c.m. of the molecule is expected, as discussed previously, to have a minor effect on the central envelopes, however this perturbation could significantly shift the frequency of the librational satellite if the librational frequencies approach that of the oscillational frequency of the molecular center of mass. Based on a simple perturbation theory argument, it can be concluded that if the translational level is above the librational state then the satellite frequency will shift to the red and vice versa.

It should also be noted that for shallow potentials, it is not possible to discuss librational satellites since the motion of the molecule is strictly rotational even though hindered (faster rotation at the valleys and slower at the hills of the potential). Thus, in the $10B$ spectrum, it is not possible to identify a librational satellite while in the $50B$ spectrum, the structure 20 cm^{-1} to the blue of the central line can be regarded as the emergence of librational motion.

Finally, it is important to consider the effect of temperature on these predicted spectra. A complete analysis of the temperature dependence requires knowledge of the temperature dependence of V^J both in the ground and excited vibrational levels of the molecule. If one assumes Flygare's interpretation of the rotational barrier, V^J depends on the molecular hexadecapole moment, which is independent of T, and the fourth gradient of the lattice potential at the molecular c.m., which depends on the cavity size and rigidity which in turn depend on T. This is an exceedingly difficult quantity to calculate and therefore is left as a model parameter. As a first approximation, ignoring the temperature dependence of V^J, the $50B$ and $100B$ spectra of Fig. 2 are reconstructed in Fig. 3 for 3, 10, and 40 K. Since the highest resolution of the instrument used in our experimental measurements is 0.06 cm^{-1}, the spectra

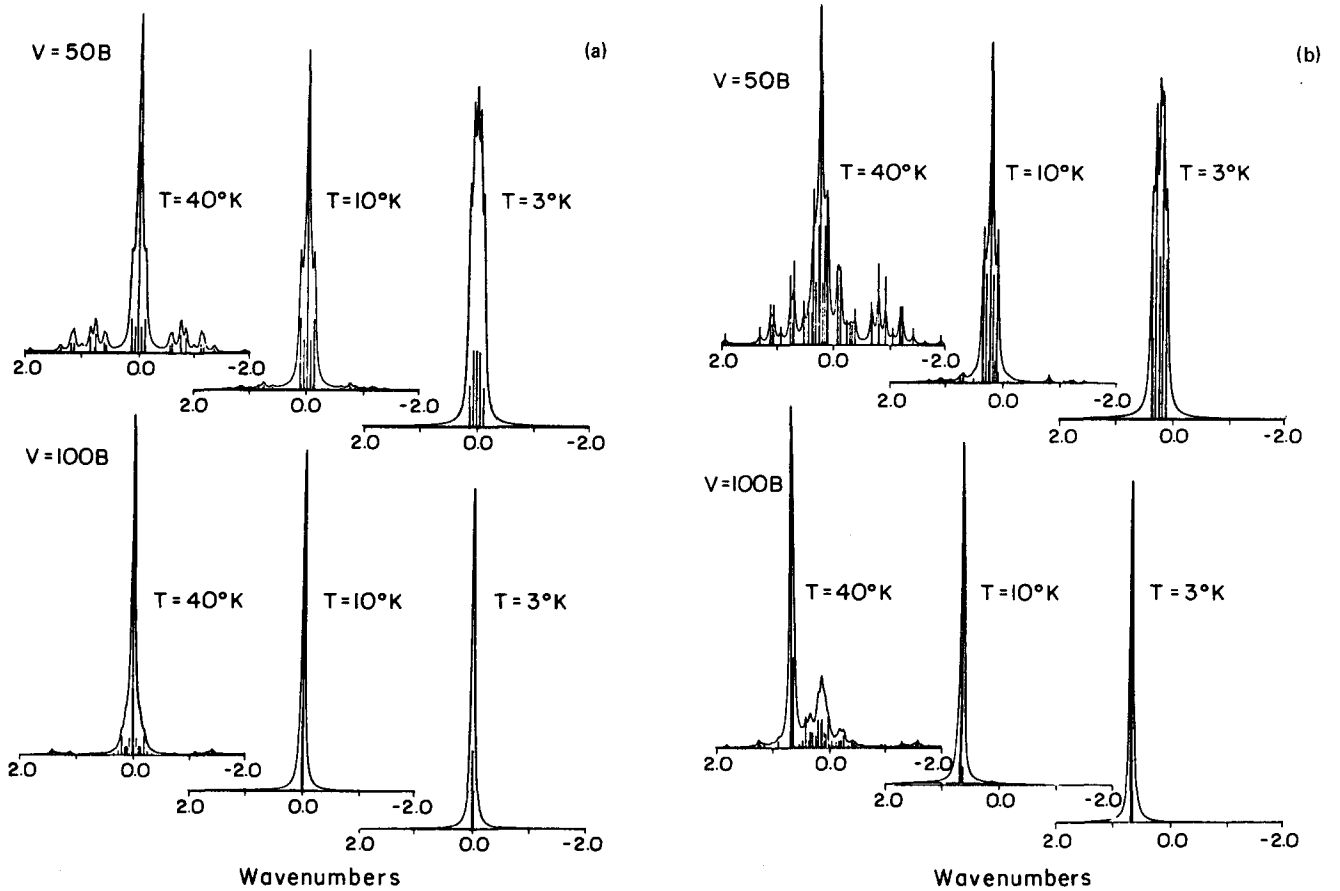

FIG. 3. Each subfigure shows the generated stick spectra for a symmetric top with $V^K = 0$, $V^J = V^{J'} = V$ as a function of temperature. In Fig. 3(b), (the right-hand set of spectra) $B' \neq B$ and $A' \neq A$. The values of Ref. 38 are used for these quantities. In each case, Lorentzians of 0.06 cm^{-1} width are superimposed on the stick spectra. In Fig. 3(a), one ordinate scale is used for the stick spectra, however, all envelopes are normalized to the same height. In Fig. 3(b), both stick spectra and envelope are normalized to the same height.

are generated assuming Lorentzians of this linewidth for the individual transitions. These finite linewidth spectra are superimposed on the stick spectra in Fig. 3. As can be seen in Fig. 3, for large values of V^J, $V^J > 50B$, the transitions coalesce under our highest resolution conditions. Thus, it is more appropriate to discuss the temperature dependence of this envelope. It should be noted that if the linewidths are truly instrument limited, then in FTIR spectroscopy their shapes will depend on the particular transformation algorithm used. As an example, if boxcar apodization is used, then $\sin x/x$ would be a more appropriate choice for the line shape, however, this detail will not affect the following discussions. Furthermore, it has been recently shown in diode-laser spectroscopic studies of CO isolated in Ar matrices that homogeneously broadened individual vibration-rotation transitions are of the order of 10^{-3} cm^{-1} which is dominated by an inhomogeneous width of 0.022 cm^{-1} in dilute annealed matrices.[37] This supports the belief that at the 0.06 cm^{-1} resolution of the FTIR individual rovibrational transitions are not resolved, but rather the overall envelope of rovibrational transitions is recorded. Thus, whether the source of coalescence is due to linewidths of individual transitions or the instrumental resolution, it is appropriate to discuss the rovibrational envelopes in comparisons of model with experiment.

The central envelopes in Fig. 3 are nearly Lorentzian. This is due to the staircase progression of intensities of transitions to either side of the Q line and not due to the assumed Lorentzian character of the individual transitions. The overall line shape is only slightly asymmetric due to the difference in intensities of P and R type transitions. At 3 K the Q line intensity drops below the intensities of transitions in the $K=0$ manifold and, thus, the center line splits. This splitting is obvious in the $50B$ case, however, cannot be resolved in the $100B$ case. At higher temperatures, the center line intensity is mainly due to the Q line and therefore the FWHM is slightly larger than 0.06 cm^{-1}. At 3 K, a larger FWHM is obtained since now the linewidth is determined by the spacing between the lowest levels of the $K=0$ manifold. The peak heights of the envelope at 10 and 40 K are nearly three or two times as large, respectively, as the peak height at 3 K. Finally, if the envelopes in Fig. 3 were fitted to either Lorentzians or Gaussians, two superimposed peaks would be sufficient to reproduce the $100B$ spectrum. The need for two peaks is best evident in the $100B$ 40 K spectrum.

The dominant feature of the spectra discussed above is due to the very strong Q line. It is well known that if the rotational constants of the ground and vibration-

ally excited states are different, then the Q line becomes a progression, the larger the spacing between rotational levels, the larger the span of the Q branch. The A and B rotational constants of CH_3F have been measured for the ground and $\nu_3 = 1$ states in the gas phase.[38] These values were used to reconstruct the spectra in Fig. 3. It should be emphasized that a difference in rotational constants of the ground and excited states is equivalent to assuming different values of V^J for these two states. The major effect of this on the spectra is the development of a pronounced asymmetry in the overall envelope—a red tail and shift of the spectral line center to the blue. These effects are accentuated as V^J is increased. This occurs because the relevant parameter for calculating energy levels is V^J/B. Thus, for a given fractional difference in B values of two vibrational levels, larger spectroscopic effects will be observed for V^J large as opposed to V^J small, since spectroscopic observations reflect the absolute difference in the energy levels of the two states. Finally, since significant shifts of vibronic line center can be produced by the difference in rotational constants, or equivalently in the rotational barrier of the initial and final vibrational states, these factors should be considered in the prediction or interpretation of observed IR matrix shifts.

The above temperature effects are basically due to variations in thermal populations of different states. There could be significant dynamic thermal effects which cannot be directly accounted for by an electrostatic model. Line broadening is perhaps the most important of these effects. In the crystal field model, both cage atoms and the trapped molecule are assumed to be fixed in position, however, since both atoms and molecule undergo oscillatory motions about their equilibrium positions, the assumed trap-site symmetry will deviate from octahedral. As long as this deviation is not large, its main effect will be that of broadening the individual transitions. If the cage were assumed rigid, this effect could be regarded as broadening due to RTC and would contribute to the homogeneous linewidth of the molecule. There could be many sources of dynamical processes that could cause temperature dependent line broadening effects—rotational relaxation in the phonon bath, motional averaging, rotational and vibrational dephasing by either direct mechanisms or with phonon or libron assistance, long range Förster type near resonant vibrational energy diffusion which in turn could proceed by different mechanisms such as direct, Raman, or Orbach processes and, finally, tunneling between the different minima of the octahedral potential (six or eight depending on the sign of V^J) which would depend on the rotational level and could be fast as long as a major distortion of the symmetry is not induced by the rearrangement of the cage atoms. These are all possible sources of dynamical line broadening. Whether the contributions of these different broadening mechanisms can be sorted out and tested is questionable, however, they are bound to contribute to some extent to the overall phenomenological linewidth of the transitions and determine much of their temperature dependence.

The model predictions and possible dynamic effects will be further discussed in the light of experimental data to be presented below.

EXPERIMENTAL

All rare gases were obtained from commercial suppliers at stated purities of > 99.995% and were used without further purification. CH_3F was obtained from Matheson at a stated purity of > 99% and was subjected to multiple freeze–pump–thaw cycles prior to mixing. Mixtures were prepared in flamed glass bulbs by standard manometric techniques using a capacitance manometer.

A closed cycle cryostat (Air Products, Displex CS-202) with a silicon diode triggered temperature controller was used. The lowest temperature achieved by the cryostat was 9 K and temperature control was nominally accurate to within ± 0.1 K. Two sets of thermocouples were used at all times, one attached to the cold trip and one embedded in the substrate. The temperature differential between the two junctions was ~1 K at the lowest temperatures. A CsI window was used as the substrate and salt windows–NaCl, KCl, or KBr—were fitted by O-ring seals to the cryohead. The background pressure for the system when cold was $\sim 10^{-6}$ Torr. Matrices were pulse deposited from a 2 ℓ reservoir. The reservoir pressure ranged between 300–700 Torr. The dead volume between the serial deposition valves was ~3 cc. Pulse rates varied, 3/min being typical.

All spectra were recorded in the transmission mode on a Fourier transform infrared spectrometer (Nicolet 7000 series), which is capable of 0.06 cm^{-1} resolution. The actual resolution of the instrument depends on the alignment of the interferometer. Normally, no special effort was exerted to purge the instrument since the region of interest ~1000 cm^{-1} is clear from atmospheric absorptions. Due to the small wedge angle of the beam splitter, interference fringes with a characteristic wavelength of 0.195 cm^{-1} are observed in high resolution spectra of optically thin samples. These could be eliminated by generating a straight line through the responsible interference peak without any deleterious effects on the remaining spectrum. The highest resolution spectra were obtained without apodization.

RESULTS

The ν_3 region and the spectral baseline over a 500 cm^{-1} bandwidth are shown in Fig. 4 for a 1:10 000 CH_3F:Kr matrix at 9 K. The matrix was deposited at 23 K and the temperature lowered to 9 K for the first trace, the second trace was obtained after annealing the matrix at 40 K for 45 minutes and lowering the temperature to 9 K. The baseline oscillations, commonly referred to as channeling, are due to constructive and destructive interference caused by the matrix interfaces. The thickness of the matrix can be obtained directly from the fringe wavelength as

$$d = \lambda/2n \ , \tag{11}$$

where λ is the channel wavelength and n is the refractive index of the matrix.

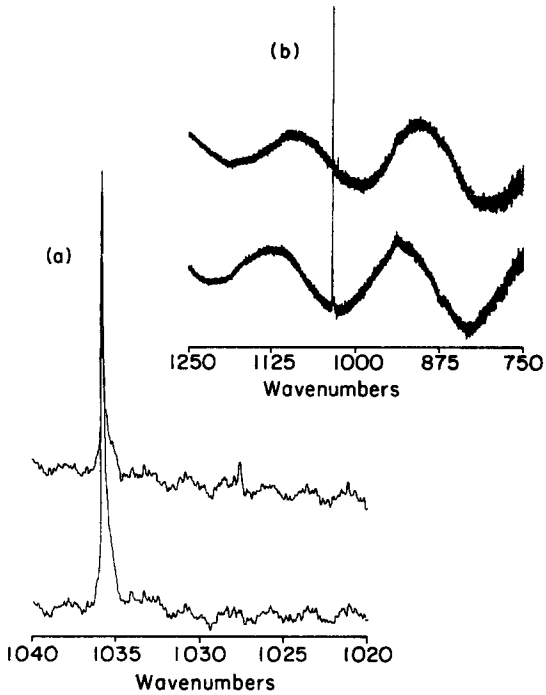

FIG. 4. The two spectral traces in the lower part of the figure (a) are for the ν_3 mode of CH_3F in a 1/10 000 M/R matrix at 9 K. The lower trace in both (a) and (b) is before annealing, the top traces are recorded after annealing at 40 K. The top of the figure (b) shows the channeling for both of the lower matrices which allows determination of the matrix thickness. In each case, the thickness is 19.8 ± 0.3.

To facilitate comparison with other work,[1] 1.34 is used for n in Kr,[39(a)] however it should be noted that 1.38 may be a better value at 10 K.[39(b)] Thus, $d = 19.8 \pm 0.3$ μ for the matrix from which the spectrum in Fig. 4 was obtained. This direct method of thickness measurement is, however, limited to thickness of the order of infrared wavelengths, typically ~5–30 μ in our near IR measurements. In thicker matrices, bulk scattering dominates and channeling cannot be observed. Figure 4 also demonstrates the development of the dimeric band and smoothening of the fringes [Fig. 4(b)] upon annealing of the matrix.

A sticking coefficient θ defined as the fraction of gas freezing on the substrate window, can be obtained from the direct measure of thickness and a knowledge of the amount of gas deposited for a given matrix. The value of θ thus obtained is particular to the given set of experimental conditions—deposition geometry and temperature, pulse size and rate, etc. However, it is quite constant throughout a given experiment. This is directly verified in the case of thin matrices from the linearity of the plot of thickness vs amount deposited [see Fig. 5(a)]. The constancy of θ for thicker matrices is verified by a more indirect method. The spectral intensity of ν_3 is integrated over a narrow bandwidth ~7 cm^{-1} and plotted vs amount deposited, yielding a linear plot which extends to the region where thickness cannot be directly measured [see Fig. 5(b)]. The integration is carried out over the same bandwidth each time by generating a straight baseline between the initial and final wavelength limits of integration. The measurements are carried out prior to annealing. Thus, from a knowledge of the thickness of thin matrices and from the plot of integrated intensity vs amount deposited the thickness of all matrices can be obtained. This is the basis of all reported thicknesses. In the experiment from which the data of Fig. 5 were compiled, θ was obtained as 0.73 ± 0.06, which is a typical value under our experimental conditions.

Clearly, from an accurate knowledge of matrix thickness and gas composition, the integrated absorption coefficient and radiative lifetime of an observed mode can be obtained. For this purpose, the integration should be carried out over a bandwidth large enough to encompass anticipated phonon wings and aggregates. Thus, a well-defined baseline is essential. This can only be achieved in thick matrices after ratioing the sample spectrum with a background containing a pure Kr matrix of similar thickness. Such a spectrum is shown

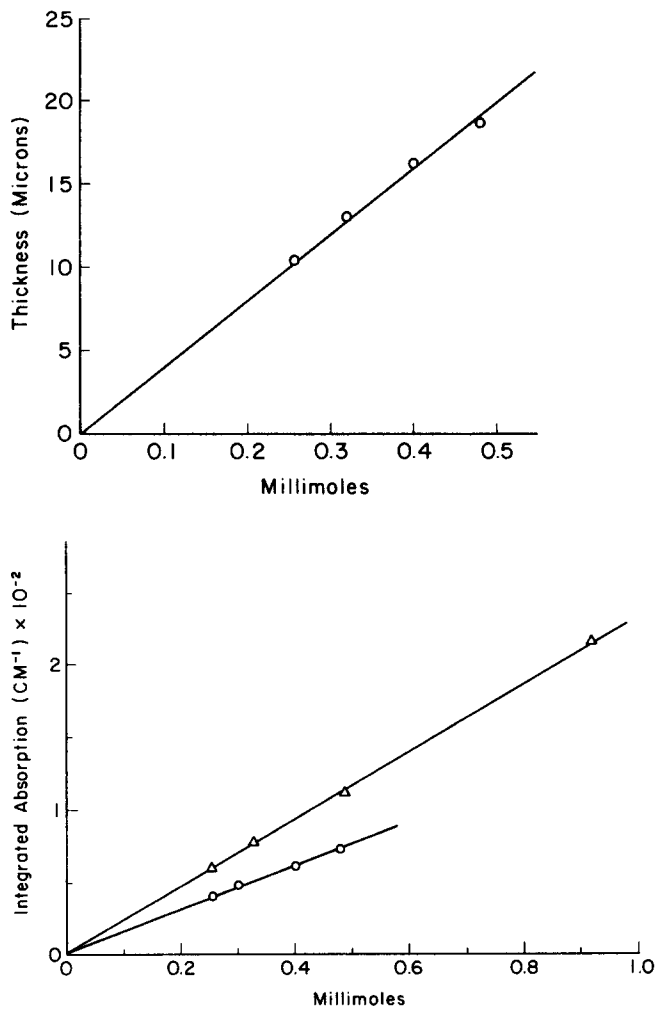

FIG. 5. (a) Thickness vs material deposited for a M/R = = 10 000 : 1 CH_3F/Kr matrix deposited at 23 K. Thickness was measured directly from the number of fringes with no heat cycling. (b) The upper points (Δ) are the data of Fig. 5(a) replotted as integrated absorption coefficient vs millimoles of gas. The integration was done over a narrow bandwith (7 cm^{-1}). The lower points (o) are for a different matrix of the same composition as in Fig. 5(a), but now recorded at 9 K.

in Fig. 6. The integration is carried out over a ~150 cm^{-1} region (950–1100 cm^{-1}) and the integrated absorption coefficient for ν_3 is obtained as[40]

$$S = \frac{c}{N}\frac{\int k_\nu d_\nu}{d} = 450\ (\pm 50)\times 10^{-9}\ cm^2\ s^{-1}\ molecule^{-1} \qquad (12)$$

and a radiative lifetime of

$$\tau = \lambda^2/8\pi S = 0.08 \pm 0.01\ s\ , \qquad (13)$$

where $\int k_\nu d_\nu$ is the integrated absorption in units of cm^{-1}, d is the matrix thickness, c is the speed of light, N is the number of CH_3F molecules in a unit matrix volume $= 2.97\times 10^{18}\ cc^{-1}$ for $M/R = 10^4$, and λ is the wavelength of the ν_3 absorption.

The ν_3 absorption region in dilute matrices is basically composed of a single intense and sharp line, which can be assigned to the isolated monomeric absorption, and much weaker lines, to the red of the monomeric absorption, which can be assigned to aggregates. In what follows, we present the assignments and detailed observations of temperature and annealing dependence of these lines.

At the deposition temperature, 22 K, and prior to any heat treatment, an intense monomeric peak appears at 1035.6 cm^{-1} with a FWHM of 0.3–0.45 cm^{-1}. A narrower line is observed when the matrix is deposited at 20 K using larger pulse sizes while a broader line is observed when deposited at 26 K using smaller pulse sizes. In each case, the line is asymmetric with a long red tail which shows characteristic broad peaks at 1034 and 1032 cm^{-1} (see Fig. 7). When cooled to 9 K, the red shoulders remain, the blue edge sharpens, and the monomeric peak shifts to 1035.87 cm^{-1} with a FWHM of 0.23–0.33 cm^{-1}. After annealing the matrix at 36 K, the monomeric peak maintains its width, the red shoulders weaken, and very weak absorptions at 1027.7, 1022.1, 1016.6, and 1008 cm^{-1} can be identified. Upon annealing at 40–45 K and cooling to 9 K, the red tail disappears and the center line narrows

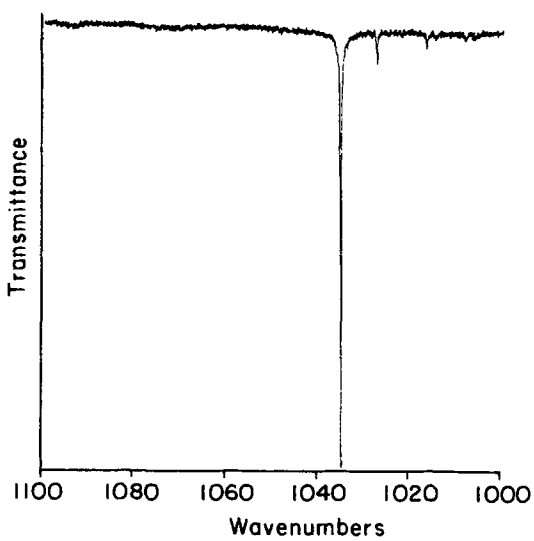

FIG. 6. $M/R = 10000:1$ CH_3F/Kr matrix annealed at 40 K, recorded at 9 K.

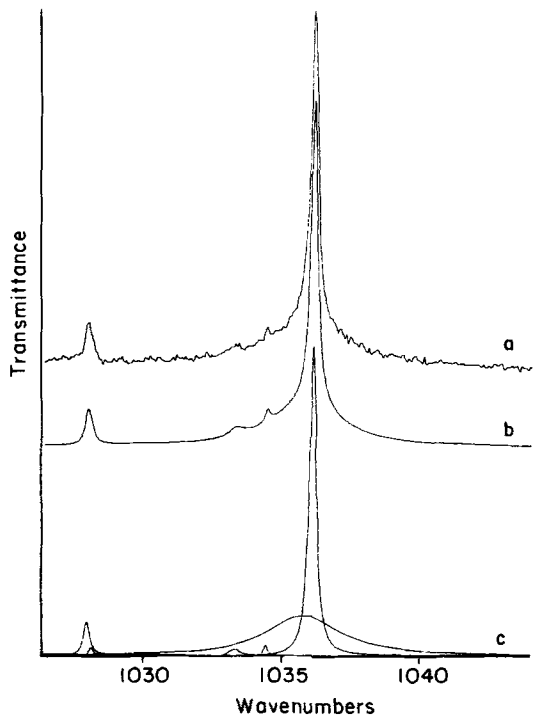

FIG. 7. $M/R = 10000:1$ CH_3F/Kr matrix. (a) shows the recorded spectrum of the matrix deposited at 23 K before any temperature cycling. (b) shows a match to the experimental spectrum by means of a sum of Lorentzians. (c) shows the widths, amplitudes and positions of the Lorentzians that go into (b).

to 0.095 cm^{-1}. However, a slight asymmetry remains on the red edge of the main peak. Simultaneous to the disappearance of the red tail is the appearance of well formed absorptions at 1016.7, 1022.1, and 1027.7 cm^{-1}.

After annealing, the 1027.7 cm^{-1} peak splits into two well separated components at 1027.6 and 1027.9 cm^{-1}. The loss in intensity of the red tail relative to the total intensity can be well correlated to the sum of intensities at these three positions. The absorption at 1027.7 cm^{-1} has been previously assigned to the dimer. The 1022, 1016, and 1008 absorptions are assigned to trimer, tetramer, and pentamer, based on the observation that in concentrated matrices after annealing at 45 K, they become very intense (see Fig. 8). An overall drop in intensity of the observed peaks accompanies the annealing process, without any loss of matrix. The latter observation is verified by annealing a 20 μ matrix at 40 K and comparing the fringe wavelengths and integrated absorptions before and after annealing (see Fig. 4). While the thickness remained unaltered, the overall intensity of the peaks was reduced by ~20%. This observation applies to thick matrices as well. However, when the integration is carried over a 150 cm^{-1} bandwidth, the loss is smaller, ~10%. Finally, an anomalous, narrow peak, FWHM ~0.09 cm^{-1} is observed at 1034 cm^{-1} after annealing the matrix above 35 K. It was noticed that in all cases when this peak was intense, the matrix was visually very porous. When these matrices were overcoated with a layer of pure Xe or pure Kr, the 1034 cm^{-1} line lost intensity. Furthermore, the 1034 cm^{-1} line could be generated by code-

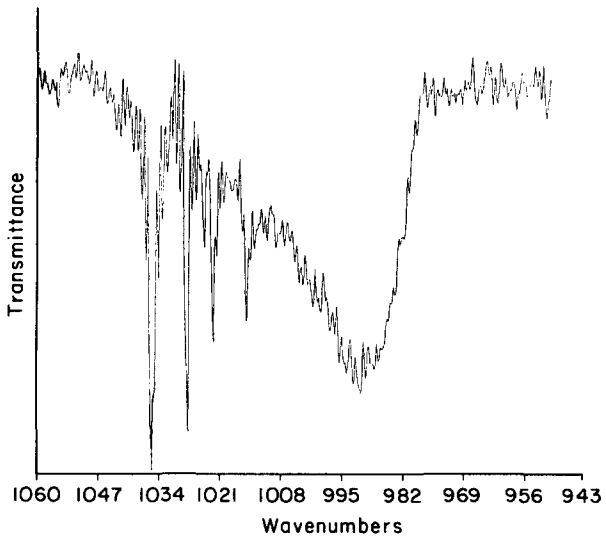

FIG. 8. An M/R of 500:1 for CH_3F in Kr deposited at 23 K and subjected to extensive annealing at 55 K.

positing N_2 in the matrix at 22 K and evaporating the N_2 at 30 K leaving behind a matrix which was very porous in appearance. A Kr matrix when overcoated with Xe could be annealed for short times at as high as 60 K without any appreciable loss of material. However, no new peaks could be observed in these experiments, thus no evidence of molecular diffusion from the Kr to the Xe bulk is observed even at these elevated temperatures. When the temperature of the overcoated and annealed matrix is lowered, the 1034 cm^{-1} line disappears and no further aggregation is observed even on further heat cycling. When the matrix temperature is kept at 65 K for a long time, the bulk of the Kr evaporates leaving behind the solid Xe overcoat which is now very porous in appearance and highly scattering.

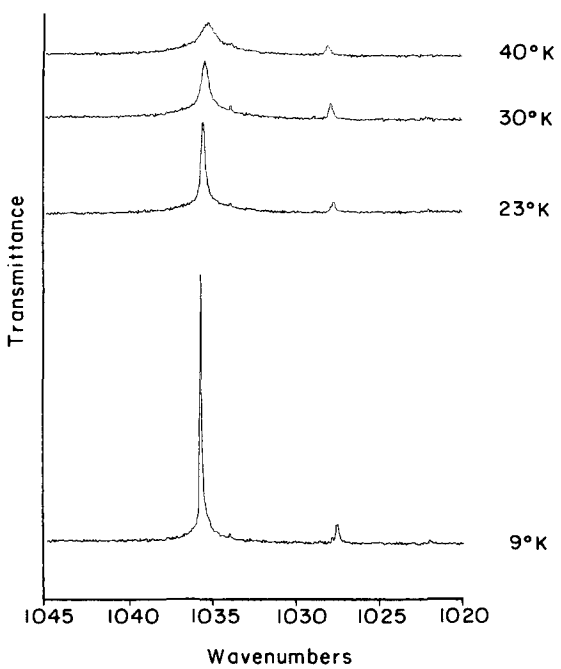

FIG. 9. The traces are for a M/R of 10 000:1 CH_3F in Kr matrix deposited at 23 K, annealed at 45 K and recorded at the indicated temperatures. All four spectra are recorded on the same ordinate scale.

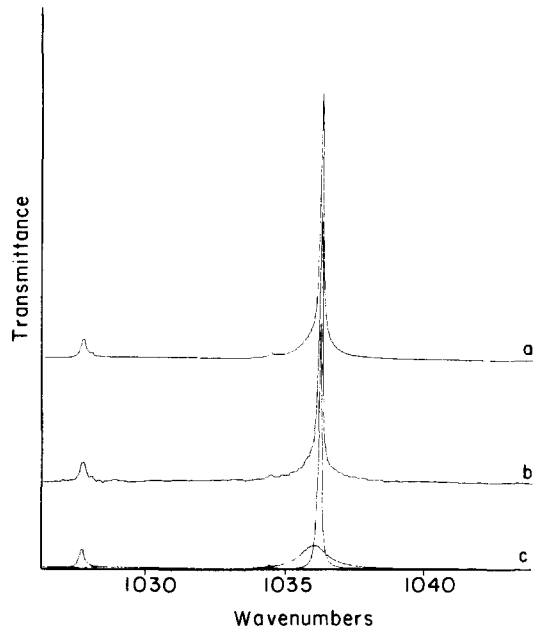

FIG. 10. The spectrum depicted is for the same matrix used to generate Fig. 7. The matrix was annealed at 45 K and the spectrum recorded at 9 K. (b) is the actual recorded spectrum, (c) is the resolution of this spectrum into Lorentzians, and (a) is the spectrum generated from the summed Lorentzians depicted in (c).

Perhaps the most striking observation is the reversible line broadening and shifting of the different peaks as a function of temperature. The monomeric line broadens by a factor of 15 between 9 and 45 K and shifts to the red by ~0.5 cm^{-1}. The dimeric doublet coalesces and shifts to the blue by ~0.5 cm^{-1} over the same temperature range, while the 1034 cm^{-1} line changes very little (see Fig. 9). In order to characterize these line shapes and their behavior, the spectrum between 1050 and 1025 cm^{-1} was fitted by the minimum number of curves necessary to reproduce the experimental spectrum. The computer program utilized could generate Gaussians or Lorentzians or lines of mixed character with the limitation that all generated lines have the same character. An excellent fit was obtained when the monomeric line was reproduced by two Lorentzians shifted with respect to each other, examples are provided in Figs. 7 and 10. In Fig. 11, the linewidth and line shift of monomeric and dimeric peaks are presented as a function of temperature.

The anharmonicity shift is an important parameter in $V-V$ energy transfer studies[8]; thus, while no attempt was made at recording spectra of modes other than ν_3 in these experiments, $2\nu_3$ was searched for and identified at 2055.65 cm^{-1} in a 10 000:1 Kr/CH_3F matrix recorded at 9 K.

DISCUSSION

The radiative lifetime of ν_3 in the gas phase is well known.[41] Numerous expressions have been derived to

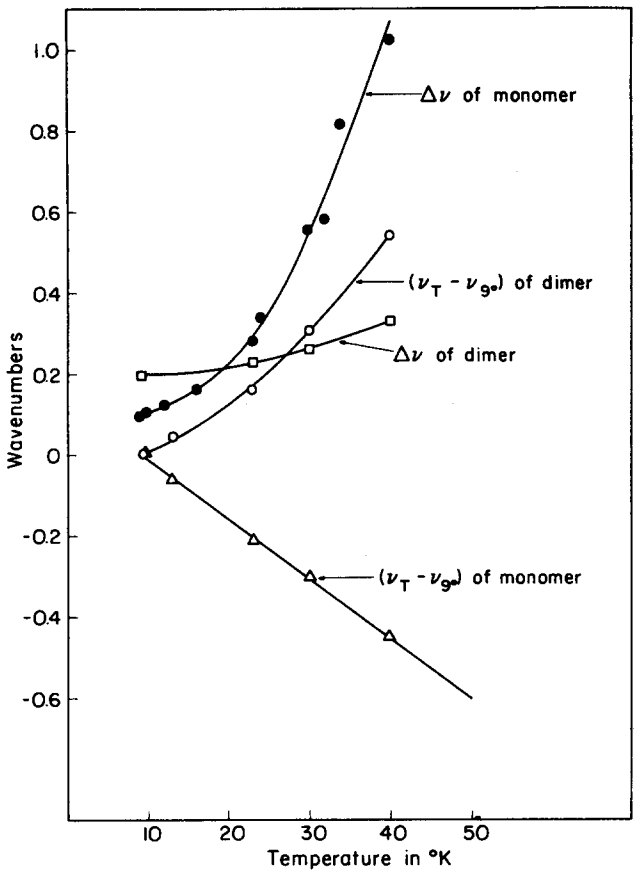

FIG. 11. Change in linewidth for the narrow monomer peak (●) shown in Fig. 10 and the principle dimer peak (□) in Fig. 10 as a function of temperature for a 10 000 : 1 CH_3F in the matrix. The reference temperature is 9 K. Also shown as ($\nu_T - \nu_{9^\circ}$) is the line shift of the narrow monomeric (Δ) and the line shift of the principle dimer peak (○). Prior to recording spectra at the indicated temperatures, the matrix was annealed at 45 K.

scale lifetimes from the gas to the condensed phases.[42] Basically, these expressions account for the difference in dielectric constant or refractive index of the two media. A commonly adopted expression is[1]

$$\tau_s = \frac{9}{n(n^2+2)^2}\,\tau_g\,, \tag{14}$$

where τ_s and τ_g are the radiative lifetimes in the solid and gas phases respectively, and n is the refractive index of the condensed medium. Therefore, in denser media, a decrease in lifetime is expected. For ν_3 of CH_3F, $\tau_g = 70$ ms, therefore $\tau_s = 33$ ms is expected in Kr ($n = 1.34$).[1] The experimental lifetime of 82 ± 10 ms is equal, within experimental error, to the gas phase value and thus a factor of 2 longer than expected. This would imply an effective reduction of the ν_3 dipole moment derivative by a factor of $\sim \sqrt{2}$ due to specific atom–molecule interactions. A potential source of error in the experimental measurements is that of matrix scattering and poorly defined baselines. However, as can be seen in Fig. 6, careful preparation of reference samples can yield very flat baselines over a large spectral bandwidth. Another source of error is the inclusion of aggregate absorptions in large bandwidth integrations, tacitly assuming that their intensitities scale linearly with the number of aggregate molecules. To test the validity of this assumption, the monomeric and aggregate peaks are integrated separately prior and after heat cycling and the ratios of the individual intensities to the total intensity compared. In each case, the fractional loss of intensity from the monomeric peak (mostly from the red edge) agreed with the gain in intensity of the aggregate peaks within 10%. Finally, it should be noted that in our spectroscopic studies, we have not directly observed predicted phonon wings. If the phonon wing reflected the bulk density of phonons, then a linewidth of ~ 50 cm^{-1} would be expected, a width ~ 500 times broader than the monomeric line. Thus, if 50% of the ν_3 intensity was transferred to the phonon wing, a baseline flatness of one part in 1000 would be required to detect this absorption when the monomeric peak is at saturation. Thus, it perhaps is not surprising that phonon wings are not observed at the studied optical densities and this could potentially be the cause of the apparently anomalously long radiative lifetime of ν_3.

The anharmonicity constant for the C–F stretching mode of CH_3F in Kr is obtained by defining the term values of the ν_3 manifold as

$$G_{\nu_3}(v) = \omega_e(v+1/2) - \omega_e\chi_e(v+1/2)^2\,,$$

from which $\omega_e = 1051.96 \pm 0.05$ cm^{-1} and $\omega_e\chi_e = 8.05 \pm 0.05$ cm^{-1} is obtained for CH_3F in Kr and at 9 K. The value for $\omega_e\chi_e$ is, within experimental error, the same as that measured for $\omega_e\chi_e$ in Ref. 6 for CH_3F in Xe matrices and is in good agreement with the gas phase value.[38]

The observation of aggregates in very dilute matrices cannot be explained on a statistical basis. In a 1/10 000 matrix, the probability that a guest molecule will be isolated with no first or second nearest-neighbor guest is $[1-(1/M/R)]^{18} = 0.9982$.[43] Thus, only $\sim 0.2\%$ of the molecules should aggregate. Contrary to this expectation, in most of our experiments with very dilute matrices ($M/R \sim 15\,000$), the dimeric peak at 1027.7 cm^{-1} can always be seen prior to any heat cycling. Furthermore, when the matrix temperature is raised to 36 K, both dimer and higher aggregate peaks intensify. In a well annealed matrix $M/R = 10\,000$, the sum of the intensities of the aggregates may be as high as 10% of the monomer intensity. Insight about the mechanisms of aggregate formation is provided by annealing and overcoating experiments. When a pulse of gas freezes at a cold surface, the released latent heat is sufficient to give a high degree of mobility to molecules at nucleation boundaries. These molecules can then migrate on matrix surfaces and aggregate. This may explain the observation that pulsed deposition usually yields a higher degree of isolation than slow spray-on.[44] In the latter case, a large area is available to molecules throughout deposition. This also correlates with the fact that the degree of isolation is quite independent of pulse size and even better with larger pulses.[44] Thus, migration on the exposed surfaces could provide a mechanism of aggregation during deposition with a larger than statistical probability. Frozen gas cannot be ex-

pected to be macrocrystalline, but rather a collection of nucleation centers with short range order, yielding inhomogeneously broadened guest absorption lines. Molecules near grain boundaries and defect centers will become mobile as the temperature of the matrix is raised.[45] The activation energy for this process will depend on the type of sites accessible to a given molecule and, therefore, is expected to have a large range of values. This is verified by the fact that matrices annealed at successively higher temperatures–between 30 and 45 K–show successively more aggregation while heat cycling between two set temperatures does not show significant further aggregation after the first cycle. Finally, the nonreversible line narrowing observed for higher annealing temperatures is symptomatic of the establishment of long range order around the isolated molecules.

The 1034 cm^{-1} line becomes clearly visible after a matrix is annealed and as a function of temperature remains rather constant in width and relative intensity. However, when the matrix is coated with a layer of pure Xe and annealed at 55 K, this line disappears and no new lines develop nor do multimeric lines further increase upon additional heat cycling. These observations lead us to postulate that the 1034 cm^{-1} line is associated with molecular absorptions at surfaces and/or grain boundaries. This postulate is further supported by the N_2 codeposition experiments. When the temperature of a codeposited matrix is raised to 30 K, N_2 evaporates leaving behind a highly porous matrix with an increased surface area. This process seems to intensify the 1034 cm^{-1} absorption. Thus, the obvious explanation for the fact that a simple geometric ratio of surface area to bulk volume is not proportional to the ratio of observed intensities of the 1034 line to that of the monomer is that the surface of the matrix is not smooth and in some cases the matrix can have a honeycomb type structure.

The fact that no new lines are observed after annealing a Xe overcoated matrix at 55 K indicates that in a well annealed matrix molecular diffusion in the bulk is minimal. The absence of further aggregation at this elevated temperature implies that aggregation occurs on the matrix surface and/or along grain boundaries.

The assignment of the 1022, 1016, and 1008 cm^{-1} lines to trimer, tetramer, and pentamer is in accord with a previous assignment for CH_3F in Ar.[25] A 500:1 matrix was prepared to test this assignment. The spectrum of Fig. 8 was obtained after extensive heat cycling of this matrix. The broad polymeric absorption at ~980 cm^{-1} is in accord with the observed absorption in pure CH_3F matrices.[20] The clear progression of these lines from monomer to polymer can be seen with near linear reduction in their intensities. The possibility that these lines belong to aggregates containing the same number of molecules, but different geometries cannot be excluded. However, their relative intensities are not correlated in dilute matrices. It is interesting to note that these aggregates show sharp absorptions distinct from the polymeric tail. This argues that aggregation does not proceed through single centered hydrogen bonding of molecules and that a finite energy minimization occurs for certain geometries of aggregates of as many as five molecules beyond which a distinct preferred geometry does not exist. These observations alone suggest some likely geometries.

The monomeric line shape undergoes an irreversible narrowing when the matrix is annealed and therefore the breadth of the preannealed matrix can be attributed largely to matrix inhomogeneity. However, the observed line is not Gaussian. This apparent contradiction can be resolved if the observed line is the envelope of unresolved structure situated such that even if the individual lines are Gaussian, the overall envelope remains basically Lorentzian. Such a situation is predicted by the electrostatic model for the case of high rotational barriers. The persistent asymmetry of the peak at low temperatures and after annealing, in the form of the red tail, is also predicted by the electrostatic model when the difference in rotational constants of the ground and excited states is included in the calculation. The observed red shift of the monomeric peak as a function of temperature can be explained by the model either as a reduction of the overall rotational barrier height or as a reduction in the difference of the rotational barrier in the excited and ground vibrational levels of the molecule as a function of temperature. Line shifts are very sensitive to the latter factor for strongly hindered molecules. As an example, it can be concluded from Fig. 3 that at $V^J = 100B$ a 5% change in relative values of V^J for the ground and excited states produces a ~0.7 cm^{-1} shift in the line center. Thus, the observed ~0.5 cm^{-1} red shift from 10 to 40 K is easily rationalized. The observed broadening of the monomeric absorption line between 10 and 40 K has to be explained by dynamical processes. In general, motional broadening and exchange processes are expected to increase with temperature. Even at low temperature 10 K, the individual rotation-vibration transitions will have a finite inhomogeneous width which is expected to be sensitive to matrix preparation methods and history. The difference in the reported linewidth of the ν_3 envelope of CH_3F in this work of 0.1 cm^{-1} and in Ref. 27 of 0.3 cm^{-1} may be due to the different methods of preparation, pulsed deposition vs slow spray-on. Clearly, if this is the cause of the different linewidths, then pulsed deposition yields more homogeneous matrices.

Reference 27 reports that some of the absorption lines in CH_3F and CD_3F broaden and split as the temperature is lowered from 10 to 3 K. Such effects can be rationalized by the model as due to a temperature dependent change in population of rotational states. For example, in the context of the model, apparent broadening can be due simply to the loss in intensity of the Q branch of a transition. This same phenomenon can produce a splitting in the rotational envelope which, in the case of parellel transitions, would not be observed if the rotational barrier is large enough to prevent the resolution of P and R type transitions in the $K=0$ manifold. However, in the case of perpendicular transitions in prolates, $\Delta K = \pm 1$ transitions are further separated and therefore this type of splitting should be more easily observed. Effects which manifest themselves as broad-

ening and splitting have been observed in Ref. 27, where 3 K spectra of perpendicular transitions in CH_3F and CD_3F are reported. Though, in general, dynamical line broadening processes can also be involved, broadening and splitting of spectral lines can occur simply due to temperature dependent changes in rotational state populations.

Perpendicular transitions are due to nuclear motions perpendicular to the figure axis. It would be expected that these will also be accompanied by barriers to spinning motion. As long as V^K is small in the excited state, perpendicular transitions will be broad and follow the gas phase vibronic contours, however, with a higher density of lines. This is due to the fact that K mixing will allow multi-K transitions in addition to the multi-J transitions allowed by J mixing. As long as the parity of the ground state $K=0$ manifold is preserved, the transitions that can be correlated with Q branch transitions will be spread over a multiplicity of states due to the mixed K character of rotational states of the $V=1$ level. This would be expected to cause broadened transitions and, as the temperature is lowered, the multiplicity of states correlating with the free rotor Q branch states would appear as splittings in the band contour. Again, it seems that effects which behave as predicted above have been observed in Ref. 27. Of course, it would be beneficial to confirm the above qualitative predictions by exact calculations for transitions in perpendicular bands.

The features of the experimental ν_3 spectrum that can be successfully explained by this model are the very narrow linewidth at low temperature, the red shift between 10–40 K and the slight asymmetry of the peak. Unfortunately, under the studied optical densities neither the anticipated phonon wing nor the predicted librational satellite (which, e.g., would be at 1070 cm^{-1} if the barrier to tumbling were 85 cm^{-1}) can be clearly identified. However, since the predicted librational transition is within the high phonon density region, it is not unlikely that it is strongly relaxed by bulk phonons and thus efficiently broadened.

In the absence of resolved vibronic structure and with the presence of numerous model parameters, it seems superfluous to attempt an exact match between model and experiment. However, at least qualitatively, the model predictions of a strongly hindered tumbler and free spinner are in excellent agreement with the experimental data. Additionally, by qualitative comparison with the model prediction, it is possible to conclude that V^J for CH_3F isolated in Kr is certainly greater than 50 B and probably of the order of 100 B (85 cm^{-1}). The magnitude of this barrier in absolute terms seems reasonable when compared to the rotational barrier assigned to CH_4.[46] Based on an electrostatic model of a tetrahedron rotating in an octahedral field,[47] a rotational barrier of 50 cm^{-1} was assigned for CH_4 isolated in Ar.[46] Clearly, a larger barrier for CH_3F can be justified based on the lowering of the molecular symmetry and stronger electrostatic interaction of the fluorine atom.

An implication of the above interpretations is that the dominant perturbation of the molecular rotations in CH_3F ν_3 is due to reorientational forces of the matrix cage. This is in contrast with the case of hydrogen halides where the dominant perturbation has been found to be that of the coupling between the molecular rotations and translations of the molecular center of mass. This contrast perhaps holds the key to the observed reverse order of relaxation efficiencies in different rare gas matrices for HCl vs the different isotopes of CH_3F. A further implication of this conclusion is that the relaxation rates of CH_3F will be relatively insensitive to the cage asymmetry as opposed to systems where RTC is important. This is verified in vibrational relaxation studies of CH_3F isolated in mixed rare gas matrices.[48] It should however be pointed out that the vibrational relaxation models, which consider the molecular rotations as the accepting modes of energy, are not sensitive to rotational barriers in the ground states that are small compared to the vibrational frequencies.[9] This is due to the fact that the rotations concerned are the very high-lying ones which are usually above rotational barriers and unperturbed. However, rotational hindrance will effectively lower the excited vibrational level relative to the unperturbed high-lying rotational levels of the ground state and therefore should be considered in determining the smallest energy gap channel for rotational deactivation.

Finally, we consider the temperature dependent, experimental linewidths and line shifts. As previously indicated, the monomeric absorption can be resolved into two Lorentzians—even though the observed line shape is believed to be the envelope of many transitions. In Fig. 11, the temperature dependence of the narrower monomeric Lorentzian linewidth and line shift has been presented together with those of the major dimeric peak. The linewidths increase nearly exponentially with temperature, however, at very different rates; the monomeric line shift is linear and towards the red while the dimeric line shift is nonlinear and towards the blue. Dynamical dephasing processes may be a major contribution to these effects and many possible sources of such relaxation processes can be identified with independent dephasing rates contributing additively to the overall observed line shape. Whether a single mechanism is dominant can usually be tested by its characteristic temperature dependence. This method of diagnosis is complicated by the fact that many different mechanisms have very similar predicted temperature dependences. As an example, quite different models of vibrational dephasing in solids predict an exponential dependence of line broadening on temperature.[49] The application of the specialized model developed by Harris *et al.* to this system,[27] can be rejected based on the argument that both line shift and linewidth are expected to have the same dependence on T (the ratio of line shift to linewidth should be independent of T for a given line), contrary to the observed exponential line broadening and linear line shift of the monomer.[49] More general vibrational dephasing models do exist,[50] however care should be taken in applying these models in order to extract mechanistic information. A complete treatment of these

relaxation processes should include all the available degrees of freedom, which in this case consists of: libration of the molecule about its x and y axes, free spin about its z axis, internal molecular vibrations, motion of the c.m. in the matrix cage, and the bulk phonon modes. Such a detailed analysis could be very informative, however it will not be attempted here.

CONCLUSIONS

Devonshire's model of a hindered diatomic rotor in an octahedral field has been extended to the special case of a hindered symmetric top rotor. The case where only the tumbling motion, rotation about the axis perpendicular to the figure axis, is hindered is explicitly considered. Thus, more appropriately, the model that is developed may be termed a hindered symmetric top tumbler. In principle, a nonzero barrier to spinning motion can also be included in the model, however, this would require a significant increase in computational effort. The important predictions of the model are:

(1) In the case of parallel transitions of a hindered tumbler, the free rotor gas phase spectrum will collapse as a function of increasing V^J to yield a very narrow envelope the line shape and line shift of which are determined by the barrier heights in the ground and excited states. The observation of very narrow vibronic envelopes does not preclude all molecular rotations since narrowing can occur even when spin about the figure axis is not hindered.

(2) The envelope will be very nearly symmetric as long as the rotational constants and potential heights of the ground and excited vibrational states are the same. A difference in either set of parameters will cause not only asymmetry, but also a line shift which should be considered in calculations of matrix induced vibrational shifts.

(3) Since the potential barrier is basically a reorientational one, its value in the excited state will depend on the type of vibrational mode involved. Thus, a set of parameters that can reproduce the structure of a given transition is not necessarily applicable to all vibrational transitions in the same molecule.

(4) The very narrow envelopes observed at large values of V^J are due to the fact that the lower energy levels of the different K manifolds nearly parallel each other. The higher librational states deviate from this behavior. Thus, for the same values of V^J, if the K spacing is decreased, which can be accomplished by isotopic substitution, as long as the involved vibrational normal mode does not change appreciably, a broader envelope would be expected. This agrees with the observation that ν_3 of CD_3F is broader than CH_3F.

(5) In the limit of very large barriers to tumbling, the molecular motion will reduce to that of a three-dimensional oscillator and plane rotor. The quadratic progression of K states will remain for high-lying states while for states well below the rotational barrier a linear progression of oscillational levels will develop. Transitions to these latter states comprise the librational satellite. As discussed previously, unless the barrier is very high, these transitions will be very diffuse. It should also be clear that the notion of librational satellites is irrelevant for small rotational barriers (see the 10 B case in Fig. 2).

The presented model of the hindered symmetric top tumbler can successfully explain many of the spectral features observed for CH_3F if a tumbling barrier of the order of 80 cm^{-1} is assumed. (This value corresponds to Devonshire's K. This is equivalent to a well to hill height of 133 cm^{-1}.) These features include: the narrow ν_3 linewidth, its asymmetry, and the red shift as a function of temperature. The model can also at least qualitatively explain some of the observations made in Ref. 27. In particular: the fact that the ν_3 linewidth does not narrow between 10 and 3 K, the breadth and splitting of perpendicular transitions as the temperature is lowered to 3 K and the fact that ν_3 of CD_3F is broader than ν_3 of CH_3F are predicted by the model. Despite these successes of the model, an exact match of experiment and model was not attempted because of the large number of model parameters and the fact that only ν_3 was studied experimentally. However, a unique match may be possible when all the modes of CH_3F and its different isotopes are considered simultaneously.

Additional conclusions drawn from the experimental studies are: (1) aggregates occur with nonstatistical intensities and are formed mostly at grain interfaces and surfaces. (2) A sharp peak at 1034 cm^{-1} is believed to be due to the surface/interface monomeric absorption. (3) Four distinct multimeric peaks are observed aside from the broad polymeric absorption. The existence of distinct multimeric peaks could in itself suggest possible bonding geometries. (4) In these studies, the overcoating method[51] was found to be a useful tool for identification of diffusional mechanisms and attenuated further aggregation. (5) Within experimental error, the radiative lifetime is the same as the gas phase value which differs by approximately a factor of 2 from the expected value for the matrix.

ACKNOWLEDGMENTS

We gratefully acknowledge the support of this work by the National Science Foundation (CHE 79-08501) and the donors of the Petroleum Research Fund administered by the American Chemical Society. We would also like to thank the Northwestern University Materials Research Center for aid in purchasing some of the equipment used in this research under NSF grant DMR-7-03019. We have greatly benefitted from discussions with and the advice of Professor G. C. Schatz, Professor M. Ratner, and Professor R. B. Gerber. We appreciate the cooperation of Dr. B. I. Swanson and Dr. L. Jones in communicating to us their unpublished results. We also thank the Northwestern University Vogelback Computer Center.

[1] F. Legay, in *Chemical and Biochemical Applications of Lasers*, edited by C. B. Moore (Academic, New York, 1977), Vol. 2.
[2] V. E. Bondybey and L. E. Brus, Adv. Chem. Phys. **41**, 269 (1980).

[3]J. T. Yardley, *Introduction to Molecular Energy Transfer* (Academic, New York, 1980).
[4]L. Abouaf-Marguin, H. Dubost, and F. Legay, Chem. Phys. Lett. **22**, 603 (1973).
[5]L. Abouaf-Marguin, B. Gauthier-Roy, and F. Legay, Chem. Phys. **23**, 443 (1977).
[6](a) V. A. Apkarian and E. Weitz, Chem. Phys. Lett. **76**, 68 (1980); (b) V. A. Apkarian and E. Weitz, Physical Chemistry Division Abstract No. 186, Las Vegas ACS Meeting, August, 1980; (c) V. A. Apkarian and E. Weitz, Third International Meeting on Matrix Isolation, Nottingham, July, 1981.
[7]L. Young and C. B. Moore, J. Chem. Phys. (to be published).
[8](a) B. Gauthier-Roy, L. Abouaf-Marguin, and F. Legay, Chem Phys. **46**, 31 (1980); (b) L. Abouaf-Marguin and R. Gauthier-Roy, Chem. Phys. **51**, 213 (1980).
[9]R. B. Gerber and M. Berkowitz, Phys. Rev. Lett. **39**, 1000 (1977); Chem. Phys. Lett. **49**, 260 (1977); M. Berkowitz and R. B. Gerber, Chem. Phys. **37**, 369 (1979).
[10]K. F. Freed and H. Metiu, Chem. Phys. Lett. 48, 262 (1977); K. F. Freed, D. L. Yaeger, and H. Metiu, *ibid.* **49**, 19 (1977).
[11]A. J. Barnes, in *Vibrational Spectroscopy of Trapped Species*, edited by H. E. Hallam (Wiley, New York, 1973), Chap. 4.
[12]A. F. Devonshire, Proc. R. Soc. London Ser. A **153**, 601 (1936).
[13]W. H. Flygare, J. Chem. Phys. **39**, 2263 (1963).
[14]W. J. Jones and N. Sheppard, Trans. Faraday Soc. **56**, 625 (1952).
[15]M. V. Mathieu, N. Sheppard, and D. J. C. Yates, Z. Elektrochem. **64**, 734 (1960).
[16]H. M. Nelson, J. Phys. Chem. **66**, 1380 (1962).
[17]W. K. Glass and A. D. E. Pullin, Trans. Faraday Soc. **59**, 25 (1963).
[18]H. E. Hallam and T. C. Ray, Trans. Faraday Soc. **59**, 1983 (1963).
[19]M. O. Bulanin and M. V. Tonkov, Opt. Spectrosc. (USSR) **16**, 234 (1964).
[20]D. A. Dows, J. Chem. Phys. **29**, 484 (1958).
[21]M. E. Jacox and D. E. Milligan, J. Chem. Phys. **50**, 3252 (1969).
[22]S. T. King, J. Chem. Phys. **49**, 1321 (1968).
[23]F. D. Verderame and E. R. Nixon, J. Chem. Phys. **45**, 3475 (1966).
[24]D. R. Anderson and J. Overend, Spectrochim. Acta Part A **28**, 1225 (1972).
[25]A. J. Barnes, H. E. Hallam, J. D. R. Howells, and G. F. Scrimshaw, J. Chem. Soc. Faraday Trans. 2 **69**, 738 (1973).
[26]B. Gauthier-Roy, C. Alamichel, A. Lecuyer, and L. Abouaf-Marguin, J. Mol. Spectrosc. **88**, 72 (1981).
[27]L. H. Jones and B. I. Swanson, J. Chem. Phys. **76**, 1634 (1982).
[28]L. Pauling, Phys. Rev. **36**, 430 (1930).
[29]M. T. Bowers and W. H. Flygare, J. Chem. Phys. **44**, 1389 (1966).
[30]H. Friedmann and S. Kimel, J. Chem. Phys. **41**, 2552 (1964); **43**, 3925 (1965); **44**, 4359 (1966); **47**, 3589 (1967).
[31]I. Prigogine, *The Molecular Theory of Solutions* (North-Holland, Amsterdam, 1957).
[32]J. H. Jaffe, A. Rosenberg, M. A. Hirschfeld, and N. M. Gailar, J. Chem. Phys. **43**, 1525 (1965).
[33]J. L. Stretton, Trans. Faraday Soc. **61**, 1053 (1965).
[34]M. E. Rose, *Elementary Theory of Angular Momentum* (Wiley, New York, 1957).
[35]P. Sauer, Z. Phys. **194**, 360 (1966).
[36]H. U. Beyeler, J. Chem. Phys. **60**, 4123 (1974).
[37]M. Harig, R. Charneau, and H. Dubost, Phys. Rev. Lett. (submitted).
[38]S. M. Freund, G. Duxbury, M. Römheld, J. T. Tiedje, and T. Oka, J. Mol. Spectrosc. **52**, 38 (1974).
[39](a) J. Marcoux, Can. J. Phys. **48**, 1948 (1970); (b) A. C. Sinnock and B. L. Smith, Phys. Rev. **181**, 1297 (1969).
[40]A. C. G. Mitchell and M. W. Zemansky, *Resonance Radiation and Excited Atoms* (Macmillan, New York, 1934).
[41]G. M. Barrow and D. C. McKean, Proc. R. Soc. London Ser. A **213**, 27 (1952).
[42]J. Van Kranendonk, Physica (Utrecht) **23**, 825 (1957); E. Hirota, Bull. Chem. Soc. Jpn. **27**, 295 (1957); A. D. Buckingham, Proc. R. Soc. London Ser. A **248**, 169 (1958).
[43]R. E. Behringer, J. Chem. Phys. **29**, 537 (1958).
[44]R. N. Perutz and J. J. Turner, J. Chem. Soc. Faraday Trans. 2 **69**, 452 (1973).
[45]L. d'Hendecourt, F. Baas, L. J. Allamandola, and J. M. Greenberg, Third International Meeting on Matrix Isolation, Nottingham University, United Kingdom, 1981; F. Frank, W. Schulze, and F. W. Froben, *ibid.*
[46]A. Cabana, G. B. Savitsky, and D. F. Hornig, J. Chem. Phys. **39**, 2942 (1963).
[47]H. F. King and D. F. Hornig, J. Chem. Phys. **44**, 4520 (1966).
[48]W. Janiesch, V. A. Apkarian, and E. Weitz, Chem. Phys. Lett. **85**, 505 (1982).
[49]S. Marks, P. A. Cornelius, and C. B. Harris, J. Chem. Phys. **73**, 3069 (1980).
[50]R. K. Wertheimer, Chem. Phys. **45**, 415 (1980); R. Kosloff and S. A. Rice, J. Chem. Phys. **72**, 4591 (1980); D. C. Knauss and R. S. Wilson, Chem. Phys. **19**, 341 (1977); R. M. Lynden-Bell, Mol. Phys. **33**, 907 (1977); W. G. Rothschild, J. Chem. Phys. **65**, 2958 (1976); S. F. Fischer and Laubereau, Chem. Phys. Lett. **35**, 1572 (1975); R. Silbey, Annu. Rev. Phys. Chem. **27**, 203 (1976).
[51]B. I. Swanson and L. M. Jones, J. Mol. Spectrosc. **89**, 566 (1981).